STEM CELLS TRANSLATIONAL MEDICINE®

TISSUE ENGINEERING AND REGENERATIVE MEDICINE

Patient-Derived Human Induced Pluripotent Stem Cells From Gingival Fibroblasts Composited With Defined Nanohydroxyapatite/Chitosan/Gelatin Porous Scaffolds as Potential Bone Graft Substitutes

JUN JI,[a,b] XIN TONG,[a] XIAOFENG HUANG,[a] JUNFENG ZHANG,[c] HAIYAN QIN,[a,b] QINGANG HU[a]

Key Words. Reprogramming • Induced pluripotent stem cells • Autologous stem cell transplantation • Osteoblast • Differentiation • Tissue regeneration

[a]Nanjing Stomatological Hospital and [b]Nanjing Key Laboratory, Nanjing Stomatological Hospital, Medical School of Nanjing University, Nanjing, People's Republic of China; [c]State Key Laboratory of Pharmaceutical Biotechnology, School of Life Sciences, Nanjing University, Nanjing, People's Republic of China

Correspondence: Haiyan Qin, D.D.S., Ph.D., Nanjing Stomatological Hospital, Medical School of Nanjing University, Nanjing 210008, People's Republic of China. Telephone: 86-25-8362-0140; E-Mail: haiyanandrew@163.com; or Qingang Hu, D.D.S., Ph.D., Nanjing Stomatological Hospital, Medical School of Nanjing University, Nanjing 210008, People's Republic of China. Telephone: 86-25-83620101; E-Mail: qghu@nju.edu.cn

Received June 26, 2015; accepted for publication October 7, 2015; published Online First on November 19, 2015.

1066-5099/2015/$20.00/0

http://dx.doi.org/10.5966/sctm.2015-0139

ABSTRACT

Human embryonic stem cells and adult stem cells have always been the cell source for bone tissue engineering. However, their limitations are obvious, including ethical concerns and/or a short lifespan. The use of human induced pluripotent stem cells (hiPSCs) could avoid these problems. Nanohydroxyapatite (nHA) is an important component of natural bone and bone tissue engineering scaffolds. However, its regulation on osteogenic differentiation with hiPSCs from human gingival fibroblasts (hGFs) is unknown. The purpose of the present study was to investigate the osteogenic differentiation of hiPSCs from patient-derived hGFs regulated by nHA/chitosan/gelatin (HCG) scaffolds with different nHA ratios, such as HCG-111 (1 wt/vol% nHA) and HCG-311 (3 wt/vol% nHA). First, hGFs were reprogrammed into hiPSCs, which have enhanced osteogenic differentiation capability. Second, HCG-111 and HCG-311 scaffolds were successfully synthesized. Finally, hiPSC/HCG complexes were cultured in vitro or subcutaneously transplanted into immunocompromised mice in vivo. The osteogenic differentiation effects of two types of HCG scaffolds on hiPSCs were assessed for up to 12 weeks. The results showed that HCG-311 increased osteogenic-related gene expression of hiPSCs in vitro proved by quantitative real-time polymerase chain reaction, and hiPSC/HCG-311 complexes formed much bone-like tissue in vivo, indicated by cone-beam computed tomography imaging, H&E staining, Masson staining, and RUNX-2, OCN immunohistochemistry staining. In conclusion, our study has shown that osteogenic differentiation of hiPSCs from hGFs was improved by HCG-311. The mechanism might be that the nHA addition stimulates osteogenic marker expression of hiPSCs from hGFs. Our work has provided an innovative autologous cell-based bone tissue engineering approach with soft tissues such as clinically abundant gingiva. STEM CELLS TRANSLATIONAL MEDICINE *2016;5:95–105*

SIGNIFICANCE

The present study focused on patient-personalized bone tissue engineering. Human induced pluripotent stem cells (hiPSCs) were established from clinically easily derived human gingival fibroblasts (hGFs) and defined nanohydroxyapatite/chitosan/gelatin (HCG) scaffolds. hiPSCs derived from hGFs had better osteogenesis capability than that of hGFs. More interestingly, osteogenic differentiation of hiPSCs from hGFs was elevated significantly when composited with HCG-311 scaffolds in vitro and in vivo. The present study has uncovered the important role of different nHA ratios in HCG scaffolds in osteogenesis induction of hiPSCs derived from hGFs. This technique could serve as a potential innovative approach for bone tissue engineering, especially large bone regeneration clinically.

INTRODUCTION

Challenges still exist for clinical bone repairing. To date, allogenic and autologous bone grafts are the two main bone repairing methods for transplantation. However, alternative approaches should be developed because of limitations such as local immune or disease transfer problems of allogenic bone grafts and the inherent donor site constraints of autologous bone. Bone tissue engineering provides a potential promising bone repairing method. However, the suitable bone tissue engineering cell source and biomimetic scaffolds for bone regeneration remain in research [1–3].

Considered as promising tissue engineering cell sources, the stem cells included embryonic stem cells (ESCs), mesenchymal stem cells (MSCs), induced pluripotent stem cells (iPSCs), and so

forth. ESCs function as pluripotent stem cells, have the capacity to differentiate into all cell types of the body, and should be the best cell source for tissue engineering. However, ethical concerns have hindered the use of human ESCs [4]. MSCs have also been widely used for their multilineage differentiation capability and immunomodulation [5–9]. However, MSCs have a limited lifespan, and it has been difficult to obtain a sufficient quantity of MSCs for bone tissue engineering. The development of induced pluripotent stem cells (iPSCs) was a milestone for stem cell research, not only because of their unlimited self-renewal capacity and pluripotent differentiation possibility, but also because iPSCs are derived autologously from patient somatic cells, which could avoid ethical problems. Therefore, iPSCs have been a promising cell source for clinical use in bone regenerative medicine [10, 11].

iPSCs can be reprogrammed from many somatic cells [12–17]. However, for potential clinical usage, the somatic cells chosen as the best cell source to be reprogrammed into iPSCs should meet the following standards: easy derivation and few hazards. Gingival fibroblasts might be a choice because they can be isolated from abundant discarded gingival tissues of dental clinical procedures and are easily cultured and expanded.

Significant efforts have been made to synthesis biomaterial scaffolds for bone defect reconstruction and regeneration in previous decades [18–20]. The biomimetic nanohydroxyapatite/chitosan/gelatin (HCG) scaffold was one type and had the advantages of simulating the constituent components of natural bone, guiding the regeneration process, and leaving nontoxic degradation byproducts. Its porous structure facilitated cell proliferation, and the degrading process was in parallel with the process of new bone formation [21, 22]. Hydroxyapatite (HA) was the core component. HA increases composite stiffness, interconnectivity, mechanical properties, and bioactivity. Consequently, initial cell adhesion and long-term growth was promoted, and cell osteogenic differentiation was induced [23, 24]. Additionally, the change in the proportion of HA in the tissue engineering scaffold led to a profound effect on the physical structure and chemical properties, which resulted in different cell behavior and performance in vitro and in vivo [25, 26]. Compared with the HA microparticles used most often in the past, HA nanoparticles (nHA) have been increasingly used in biomaterial composites because of their excellent biocompatibility, bioactivity, osteoconductivity, and osseointegrative nature [27–30]. HCG composites with nHA promote ion exchange, increase resorbability, and facilitate new bone generation [28]. In composites, the tight integration between nHA and complex organic matrix improves the microhardness and enhances mechanical durability and bioactivity [29, 31].

Previous research has shown in short-term results that the addition of HA improves MC3T3-E1 cells' bioactivity and mineralization in vitro and bone healing potential in vivo [26]. However, for human cell-based bone reconstruction and regeneration purposes, which ratio of nHA in HCG scaffolds is most suitable in the long term is still under research. In the present study, we, first, established human induced pluripotent stem cells (hiPSCs) reprogrammed from human gingival fibroblasts (hGFs), which have enhanced osteogenic differentiation capability. Second, we defined HCG scaffolds by synthesizing and comparing 2 types of HCG scaffolds with a different ratio of nHA (HCG-111, 1 wt/vol% nHA; and HCG-311, 3 wt/vol% nHA). Finally, hiPSCs from hGFs were composed with 2 types of HCG scaffolds, and the osteogenic differentiation and new bone formation were evaluated and compared in vitro and in vivo for up to 12 weeks.

Materials and Methods

hGFs Isolation, Expansion, and Reprogramming Into hiPSCs

Discarded gingival tissue specimens from clinical surgery (3 donors: 2 women, aged 23 and 35 years, and 1 man, aged 18 years) from our hospital were collected with ethical approval. Primary hGFs were then isolated and expanded. In brief, minced gingival tissues were digested with 3 mg/ml collagenase I and 4 mg/ml dispase (Sigma-Aldrich, St. Louis, MO, http://www.sigmaaldrich.com) in a 37°C water bath for 60 minutes and then filtered with a 70-μm cell strainer (BD Biosciences, Franklin Lakes, NJ, http://www.bd.com). The isolated hGFs were seeded in a 75-ml flask (Corning Mediatech, Manassas, VA, http://www.cellgro.com) with culture media containing α-modified minimum essential medium (α-MEM; Gibco, Gaithersburg, MD, http://www.lifetechnologies.com) supplemented with 10% fetal bovine serum (FBS; Gibco), 100 μM L-ascorbic acid 2-phosphate (Sigma-Aldrich), 2 mM L-glutamine (Amresco, Solon, OH, http://www.amresco-in.com), 100 U/ml penicillin, and 100 μg/ml streptomycin (Sigma-Aldrich) in a humidified incubator at 37°C and 5% CO_2, as previously described [32]. hGFs were detached with 0.25% trypsin/EDTA (Sigma-Aldrich) and passaged when they had grown to 80% confluence. Passage 2 hGFs were prepared for reprogramming into hiPSCs.

The hGFs reprogramming was performed the same as in our previously published work [9]. Passage 2 hGFs were seeded into a 12-well plate with an allocation of 1×10^5 cells per well. Lentivirus containing four factor genes (*Oct4*, *Sox2*, *c-Myc*, and *Klf4*; Sidansai Biotechnology, Shanghai, China, http://www.sidansai.com) were used for reprogramming. Next, 1×10^7 unit virus supplemented with polybrene at 4 μg/ml was added to each well. Mouse embryonic fibroblasts were used as feeder cells. The reprogrammed hGFs were seeded onto feeder layer within 7 days after transduction. ESC-like colonies merged after 3 weeks. Each colony was manually picked in one well of a four-well plate for expansion and subcloning. hiPSCs were also cultured with feeder-free medium (EMD Millipore Corp., Billerica, MA, http://www.emdmillipore.com) in a Matrigel (BD Biosciences)-coated plate. ESC-like colonies were identified in vitro by alkaline phosphatase (AP) staining; TRA-1-60, TRA-1-81, TRA-2-49, SSEA4, and Nanog immunofluorescence staining as ESC pluripotency markers; and neuron differentiation. Standard G-banding chromosome analysis was performed in a clinical laboratory of our hospital. The hiPSC colonies reprogrammed from hGFs were analyzed for karyotyping at an earlier stage (passage 2) and later stage (passage 16). In vivo teratoma formation was performed in accordance with the protocol. The hiPSCs from approximately two to six wells of a six-well plate were collected, centrifuged, resuspended in Dulbecco's modified Eagle's medium/F12 and then intramuscularly injected into the right hind leg of a severe combined immunodeficiency (SCID) mouse for teratoma formation.

hiPSC Osteogenesis Induction In Vitro

We used 0.5 mg/ml dispase II (EMD Millipore Corporation) for hiPSC digestion. The colonies were detached from the plate, transferred to a 15-ml tube, washed, and resuspended in an ultra-low attachment six-well plate for embryoid body (EB) formation and culture. EBs were dissociated into single cells and cultured in six-well plates with hiPSC feeder-free media or induced

with osteogenesis induction media. Osteogenesis-inducing media consisted of α-MEM (Gibco) supplemented with 10% FBS (Gibco), 100 μM L-ascorbic acid 2-phosphate (Sigma-Aldrich), 2 mM L-glutamine (Amresco), 100 U/ml penicillin and 100 μg/ml streptomycin (Sigma-Aldrich), 1.8 mM KH_2PO_4 (Sigma-Aldrich), and 10^{-4} M dexamethasone sodium phosphate. The culture media were changed every 2–3 days. hiPSC induction was maintained for 21 days, and the results were analyzed using alizarin red staining.

Fabrication and Characterization of HCG Scaffolds

The nHA [$Ca_5(PO4)_3OH$] nanosize powders were purchased from Sinopharm Chemical Reagent (Shanghai, China, http://www.shreagent.lookchem.com). The morphology of the nHA (at a magnification of ×5,000 and ×50,000) was detected using a field emission scanning electron microscope (SEM; model JSM7600F; JEOL, Tokyo, Japan, http://www.jeol.co.jp), and the relative proportions of the constituent elements were determined using energy dispersive spectroscopy (EDS). The three-dimensional (3D) porous scaffolds were produced as previously described [21–23]. Different weights of nHA powder were mixed in deionized water separately to make 1 wt/vol% and 3 wt/vol% HA solutions. These were stirred for 1 hour and dispersed thoroughly by ultrasonication. Next, the following components were added into the solutions: 1 wt/vol% low-molecular-weight chitosan powder (Sigma-Aldrich), followed by 1 vol/vol% acetic acid, and 12 hours later, 1 wt/vol% type B gelatin powder (Sigma-Aldrich). The mixtures were disturbed well by an additional 12 hours of agitation before being poured into 8-mm-diameter stainless steel cylinder molds. Immediately after molding, the mixtures were frozen at −20°C for 2 hours to solidify the solvent and induce solid-liquid phase separation. After 48 hours of lyophilization, cylinder-shaped scaffolds had formed, which were later cut with a sharp blade into 5-mm-thick disks (8 mm diameter). Next, the acetic acid in the scaffolds was neutralized by 10 wt/vol% NaOH for 4 hours before a phosphate-buffered saline (PBS) wash. Dipped in 0.5 vol/vol% aqueous glutaraldehyde solution for 1 hour for cross-linking, the scaffolds were further treated with 2 wt/vol% sodium borohydride aqueous solution to neutralize the residual glutaraldehyde. Washed again in PBS, the scaffolds were then immersed in 75% ethanol for 1 hour for sterilization. Next, three changes of PBS were used to remove the ethanol. Finally, the porous HCG scaffolds were freeze dried again for use. The relative ratios (wt/vol%) of the solid contents (HA, chitosan, and gelatin) in the 2 types of HCG scaffolds were 1:1:1 and 3:1:1, denoted in the present study as HCG-111 and HCG-311, respectively (supplemental online Table 1).

The morphologic properties of the HCG-111 and HCG-311 scaffold samples were examined by SEM imaging. Central longitudinal sectioned samples were mounted on copper stubs and sputter coated with gold palladium film. The pore shape and size in the cross-sections were observed, recorded, and measured on SEM images at ×200 and confirmed by fluorescence observation and H&E staining. The average pore width within the HCG-111 and HCG-311 scaffolds were calculated separately from the intercepts in the longitudinal plane as the mean ± SD (n = 16). SEM images at different magnifications (×1,000, ×5,000, and ×50,000) were used to study the inner scaffold morphology.

Scaffold porosity was determined using the Archimedes principle [33, 34]. Distilled water was used as the displacement liquid and operated at 4°C with a density of 1.0 g/ml. Dry HCG-111 and HCG-311 scaffolds were weighed (Wd; the weight of the scaffold) separately, and then immersed in distilled water. After sonication for 5 minutes to induce pore filling and eliminate air from the scaffolds, the saturated scaffolds were weighed immersed in water (Wi; the weight of the scaffold submerged) suspended by a string. Subsequently, the saturated samples were reweighed (Ws; the weight of the scaffold filled with water) in air. The density was calculated using Equation 1:

$$\text{Density } (\text{g/mL}) = \text{Wd}/(\text{Ws} - \text{Wi}) \times \rho_{\text{w}} \quad (1)$$

The apparent porosity was calculated using Equation 2:

$$\text{Porosity } (\%) = (\text{Ws} - \text{Wd})/(\text{Ws} - \text{Wi}) \times 100\ \% \quad (2)$$

Three samples were measured for each scaffold, and the results are shown as the mean ± SD.

The adsorption characteristics indicate the scaffolds' water uptake abilities and protein adsorption differences [23, 35]. The adsorption characteristics in PBS and α-MEM (supplemented with 10% FBS) were recorded for 12 weeks. First, 3 samples each of the HCG-111 and HCG-311 scaffolds were removed from the desiccators, which were weighed (Wd) and then immersed in PBS and α-MEM (supplemented with 10% FBS) at room temperature. Next, the samples were gently blotted with filter paper to remove the excess bulk water and reweighed (Ww) to determine the water uptake at predetermined time intervals (1 and 3 days and 1, 2, 3, 6, and 12 weeks). The percentage of adsorption (EA) of the scaffolds at equilibrium was calculated using Equation 3 [30]:

$$\text{EA} = [(\text{Ww} - \text{Wd})/\text{Wd}] \times 100\% \quad (3)$$

The results are expressed as the mean ± SD.

hiPSCs Seeded Onto HCG Scaffolds and Cultured In Vitro

The scaffolds were presoaked in α-MEM with 10% FBS for 24 hours to facilitate hiPSC attachment and then placed into a 24-well culture plate. To prevent cell attachment, the plate well bottom was precoated with a thin layer of 2% agarose gel. hiPSC colonies that formed EBs were dissociated into single cells with 0.05% trypsin/EDTA (Invitrogen, Carlsbad, CA, http://www.invitrogen.com) for 5 minutes at 37°C and then cultured in 100-mm dishes with human mesenchymal stem cell culture medium containing α-MEM (Gibco) supplemented with 10% FBS (Gibco), 100 μM L-ascorbic acid 2-phosphate (Sigma-Aldrich), 2 mM L-glutamine (Amresco), and 100 U/ml penicillin and 100 μg/ml streptomycin (Sigma-Aldrich). The culture media were changed every 2–3 days. The differentiated cells were then collected with 0.05% trypsin/EDTA (Invitrogen), sorted by flow cytometry with anti-stro-1 antibody (Santa Cruz Biotechnology Inc., Santa Cruz, CA, http://www.scbt.com). Stro-1-positive cells were then slowly and evenly seeded into the presoaked HCG-111 and HCG-311 scaffolds (8-mm diameter × 5 mm thick) by syringe needles (1×10^6 cells per sample, n = 3 per group per time point). After 2 hours of incubation to allow the cells to disperse and attach inside the scaffolds, a certain volume of culture media was slowly added to the plate wells to submerge the samples. The tissues were then cultured in a humidified incubator at 37°C and 5% CO_2 for up to 12 weeks for in vitro study. Culture media were changed every 2–3 days. For in vivo research, the composites were removed and transplanted subcutaneously into nude mice after 1 week of incubation.

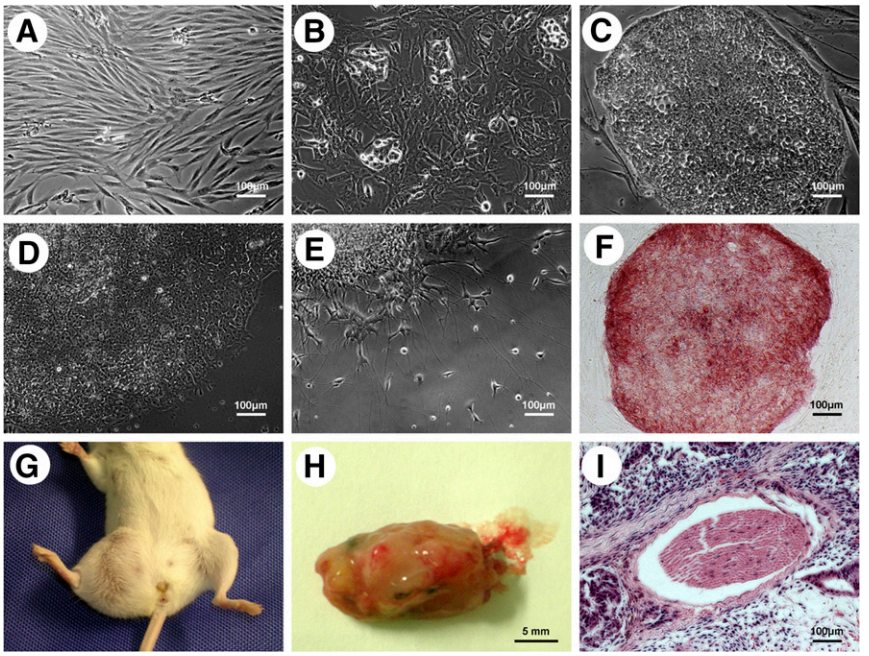

Figure 1. Establishment and characterization of human induced pluripotent stem cells (iPSCs) from human gingival fibroblasts (hGFs). **(A):** hGFs passage 2 showed spindle-like morphology. **(B):** Small cell clusters were seen at day 12 after hGFs had transfected with four lentiviruses (*Oct4*, *Sox2*, *c-Myc*, and *Klf4*). **(C):** Embryonic stem cell (ESC)-like colonies emerged within 3 weeks after hGF transfection. **(D):** The ESC-like colonies were cultured with feeder-free iPSC culture medium. **(E):** The ESC-like colonies could differentiate into neuron-like cells. **(F):** ESC-like colonies showed alkaline phosphatase-positive staining (red). **(G–I):** In vivo teratoma formed when ESC-like colonies were injected into the right hind leg of a severe combined immunodeficiency mouse intramuscularly. Scale bars = 100 μm **(A–F, I)** and 5 mm **(H)**.

SEM Examination and Histologic Staining

At predetermined in vitro cultured time points (e.g., weeks 1, 2, 4, and 12), the hiPSC/HCG complexes were removed and washed twice in PBS. After fixation in 10% formalin overnight, the samples were dehydrated using a graded ethanol series. For SEM examination, the composites were lyophilizated 48 hours before being sputter coated with gold. For histologic observation, the samples were embedded in paraffin blocks and sectioned into 5-μm-thick slices for H&E and Masson's trichrome staining.

Osteogenic Marker Expression Evaluated by Quantitative Real-Time Polymerase Chain Reaction

The samples from the two composite types were subjected to quantitative real-time polymerase chain reaction analysis to quantify the hiPSC osteogenic differentiation at 4 weeks of in vitro culture. Five osteogenic marker genes (*ALP*, *Col1*, *Runx-2*, *OCN*, and *OPN*; supplemental online Table 2) were assessed. RNA was extracted using the TRIzol reagent kit (Invitrogen) according to the manufacturer's instructions. Gene amplification was performed using Stepone plus PCR (Applied Biosystems, Foster City, CA, http://www.appliedbiosystems.com). The results were analyzed using the $2^{-\Delta\Delta Ct}$ method [36, 37], where the Ct values were normalized to the human 18S in the same sample and further normalized to the Ct values of the control HCG-111 samples. The results are expressed as the mean $\pm$ SD (n = 3).

hiPSC/HCG Complex Transplanted In Vivo

The specific pathogen-free BALB/c immunocompromised mice (male, aged 4–5 weeks, n = 12) used in the present study were purchased from Vital River Laboratories Co., Ltd. (Beijing, China, http://www.vitalriver.com). The animal research and care committee of our medical school approved the animal experiments.

The surgeries were performed under sterile conditions. Anesthesia was performed by intraperitoneal injection of 3% sodium pentobarbital (40 mg/kg) and maintained by isoflurane flow. The mouse back was disinfected with 0.5% iodophor solution, and four incisions (each 10 mm long) were made in the dorsum skin. A subcutaneous pocket was separated deeper inside each incision using scissors. Individually, four hiPSC/HCG complexes were inserted into the four dorsal subcutaneous pockets. In each mouse, an experiment group (HCG-311) and control group (HCG-111) were transplanted in a preset sequence, in an attempt to eliminate the individual differences in the mice. The incisions were then sutured in place using 4-0 suture. Pure scaffolds (HCG-111 and HCG-311) without cells were also transplanted as a blank control group. After anesthesia recovery, the mice were fed in individual cages until the cone-beam computed tomography (CBCT) images were taken, and the specimens were retrieved at 12 weeks.

3D CBCT Imaging and "Bone" Density Measurement

The CBCT images were taken using a NewTom VG scanner (QR srl, Verona, Italy, http://www.newtom.it) according to the manufacturer's protocol with a voxel size of 0.20 mm. 3D imaging and 3D rendering of the soft tissue, bone, and materials were then created using Software NNT viewer, version 5.3, in which optimal visualization of the images was obtained using the image-processing tool of the software. The Ct values of the material and mouse thighbone sections were quantitatively calculated using the density measurement tool in Software Mimics, version 10.01 (Materialise NV, Leuven, Belgium, http://www.materialise.com).

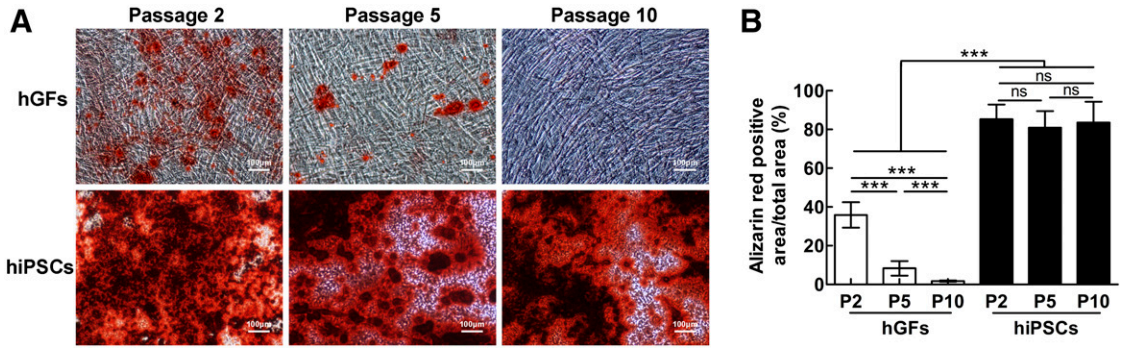

Figure 2. Osteogenic differentiation with hGFs and hiPSCs. **(A):** Alizarin red staining of hGFs (top) and hiPSCs (bottom) at passages 2, 5, and 10. hGFs showed decreased osteogenic differentiation capability as the cell passage number increased. hiPSCs presented with higher osteogenic differentiation capability and elevated calcified nodules, regardless of the passage number, compared with hGFs. Scale bars = 100 μm. **(B):** Percentage of positive alizarin red staining showed that hiPSCs had significantly increased osteogenic differentiation capability compared with hGFs. Data are presented as mean $\pm$ SD (n = 3). ***, $p < .001$. Abbreviations: hGFs, human gingival fibroblasts; hiPSCs, human induced pluripotent stem cells; ns, no statistically significant difference ($p > .05$); P, passage.

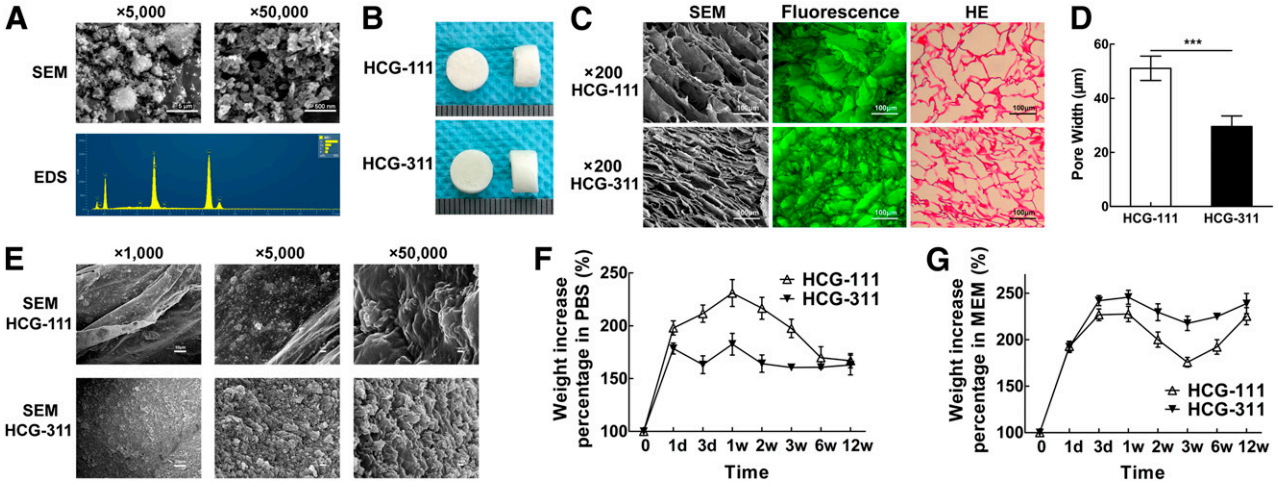

Figure 3. Characteristics and property of HCG-111 and HCG-311 scaffolds. **(A):** SEM and EDS microanalysis for HA nanoparticles. Nanohydroxyapatite (nHA) showed a rod-like nanostructures (approximately 100 nm $\times$ 30 nm) at higher magnification (scale bars = 500 nm). However, at lower magnification (scale bars = 5 μm), nHA agglomerations were rougher lumps, approximately 1–2 μm. EDS spectra were obtained with the beam focused on the nHA particles. The predominant components were carbon, oxygen, phosphorus, and calcium (carbon detected by the conductive tapes). **(B):** Photographs showing the synthesized scaffolds were 8 mm in diameter $\times$ 5 mm thick. **(C):** SEM images, fluorescence observation, and H&E staining in the cross-sections showing the inner scaffold network connection and pore structure. Scale bars = 100 μm. **(D):** The measured pore width showed that HCG-111 had larger pores than HCG-311. Data are shown as mean $\pm$ SD (n = 16, ***, $p < .001$). **(E):** SEM images at different magnifications showed the HCG-311 pore wall had rougher structures. From left to right in sequence, scale bar = 10 μm, 1 μm, and 100 nm. **(F):** Absorption characteristics of scaffolds soaked in phosphate-buffered saline (PBS) as a function of time. HCG-111 had increased more in weight within 12 weeks. Data are presented as mean $\pm$ SD (n = 3). **(G):** Absorption capacity of scaffolds soaked in α-MEM (10% FBS) was greater with more protein than that for scaffolds soaked in PBS, stratified by time. HCG-311 uptake resulted in a greater weight within 12 weeks. Data are presented as mean $\pm$ SD (n = 3). Abbreviations: d, day; EDS, energy dispersive spectroscopy; HCG, nanohydroxyapatite/chitosan/gelatin; HCG-111, HCG scaffold with 1 wt/vol% nHA; HCG-311, HCG scaffold with 3 wt/vol% nHA; HE, H&E; MEM, α-modified minimum essential medium; PBS, phosphate-buffered saline; SEM, scanning electron microscopy; w, week.

Histological Assessment (H&E and Masson) and Immunohistochemistry Staining

The specimens retrieved from in vivo transplants were fixed in 10% formalin for 48 hours, decalcified with 10% EDTA for 30 days, embedded in paraffin blocks, and sectioned 5 μm thick for H&E, Masson, and immunohistochemistry (IHC) staining.

For H&E staining, the sections were stained in hematoxylin for 5 minutes, followed by 3 s in acid alcohol for decoloration. The sections were then rinsed in Scott's tap water substitute before being stained in eosin for 1 minute. Masson staining was conducted according to the manufacturer's protocol. In brief, the sections were immersed in Weigert's iron hematoxylin and then three different solutions successively: plasma stain, phosphomolybdic acid in distilled water, and fiber stain.

IHC staining was performed with anti-osteocalcin antibody (OCG3; ab13420; Abcam, Cambridge, U.K., http://www.abcam.com) at a 1:100 dilution; for anti-RUNX-2 staining, RUNX2 (D1H7) rabbit monoclonal antibody 8486s (Cell Signaling Technology, Beverly, MA, http://www.cellsignal.com) was used according to the manufacturer's instructions.

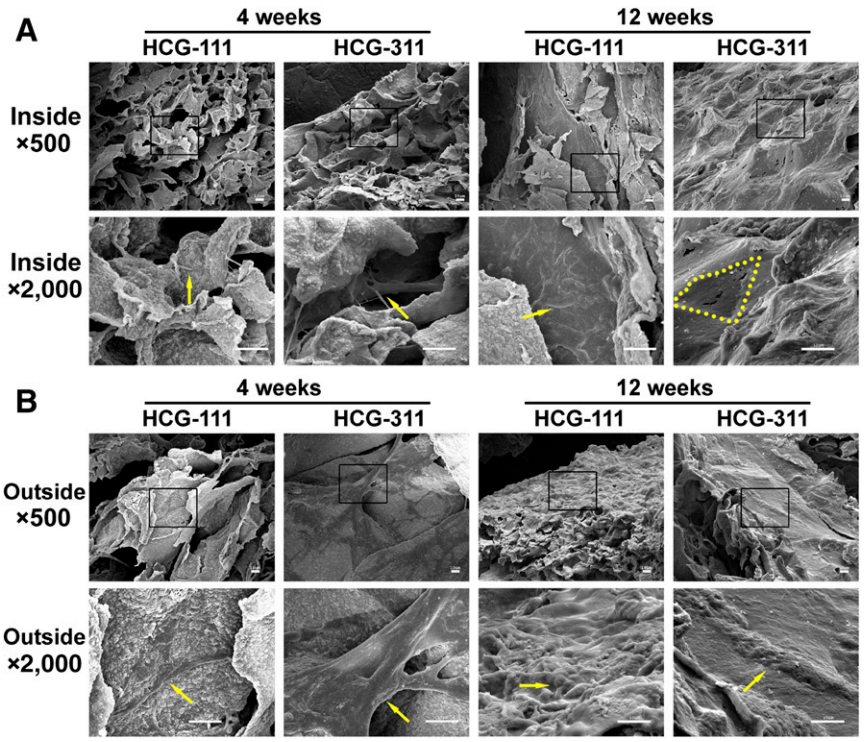

Figure 4. Scanning electron microscope (SEM) images revealing the inside and outside appearance of in vitro-cultured tissues. **(A):** Inside the HCG-111 and HCG-311 scaffolds, the cells communicated and an intercellular bridge had formed (yellow arrow) at 4 weeks. Cells and membrane had blocked the pores (yellow dots outline inside pore margin) on HCG-311 or spread out along with the pore wall (yellow arrow) on HCG-111 at 12 weeks. **(B):** Outside appearance of cell adherence and proliferation at 4 weeks (yellow arrows) and membrane formation at 12 weeks (yellow arrows) on HCG-111 and HCG-311. Higher magnification images (bottom) show an expanded view of the selected areas (black rectangles) in the top images. Scale bars = 10 μm. Abbreviations: HCG-111, nanohydroxyapatite/chitosan/gelatin scaffold with 1 wt/vol% nanohydroxyapatite; HCG-311, nanohydroxyapatite/chitosan/gelatin scaffold with 3 wt/vol% nanohydroxyapatite.

Statistical Analysis

The quantitative values are expressed using descriptive statistics such as the mean $\pm$ SD. The data were analyzed using GraphPad Prism, version 5 (GraphPad Software, Inc. , San Diego, CA, http://www.graphpad.com). Box plots were used to compare the groups. Statistical analysis was performed using one-way analysis of variance followed by Tukey's multiple comparison test to identify any differences. Differences with $p < .05$ were considered statistically significant.

Results

Establishment and Characterization of hiPSCs From hGFs

The hGFs were transduced with lentivirus containing four factor genes (*Oct4*, *Sox2*, *c-Myc*, and *Klf4*; Fig. 1). At day 12 after transduction, cell clusters were seen, and ESC-like colonies had emerged within 3 weeks. The emerged ESC-like colonies had strongly and positively stained with ES pluripotency marker AP staining. Immunofluorescence staining of other ES pluripotency markers (TRA-1-60, TRA-1-80, TRA-2-49, SSEA4, and Nanog) was also positive (supplemental online Fig. 1A). Karyotypic analysis of early and later stage merged ESC-like colonies from hGFs of 2 patients showed normal results (supplemental online Fig. 1B, 1C). These findings indicate that our reprogramming system did not alter the cell karyotype. The ESC-like colonies could also differentiate into neurons. The teratoma was well formed when the cells were injected into the right hind leg of a SCID mouse intramuscularly. EBs had developed for osteogenic differentiation. These data show that the emerged colonies were pluripotent-like ESCs; therefore, hiPSCs from hGFs were well established.

The hiPSCs from hGFs had increased osteogenic differentiation capability compared with that of the original hGFs, indicated by alizarin red staining analysis (Fig. 2). Alizarin red staining showed elevated calcified nodules of hiPSCs from hGFs.

Morphology, Density, and Porosity Properties of HCG-111 and HCG-311 Scaffolds

The representative SEM images of the nHA particles (Fig. 3A) showed rod-like nanoparticles (approximately 100 nm $\times$ 30 nm) at a magnification of $\times$50,000. However, at a magnification of $\times$5,000, the nanoparticles had agglomerated into rougher lumps of approximately 1–2 μm. With the beam focused on the nHA particles, EDS spectra were obtained, and the predominant components were found to be carbon, oxygen, phosphorus, and calcium (carbon was detected by the conductive tapes).

The different ratios of the solid components in the scaffolds (i.e., nHA, chitosan, and gelatin), porosity, and density are listed in supplemental online Table 1. The increase in nHA content significantly influenced the HCG scaffold densities, which increased from $65.1 \pm 1.6 \times 10^{-3}$ g/ml (HCG-111; 1 wt% nHA) to $103.5 \pm 2.0 \times 10^{-3}$ g/ml (HCG-311; 3 wt% nHA). However, both scaffolds showed very high porosity, greater than 93%, which was less

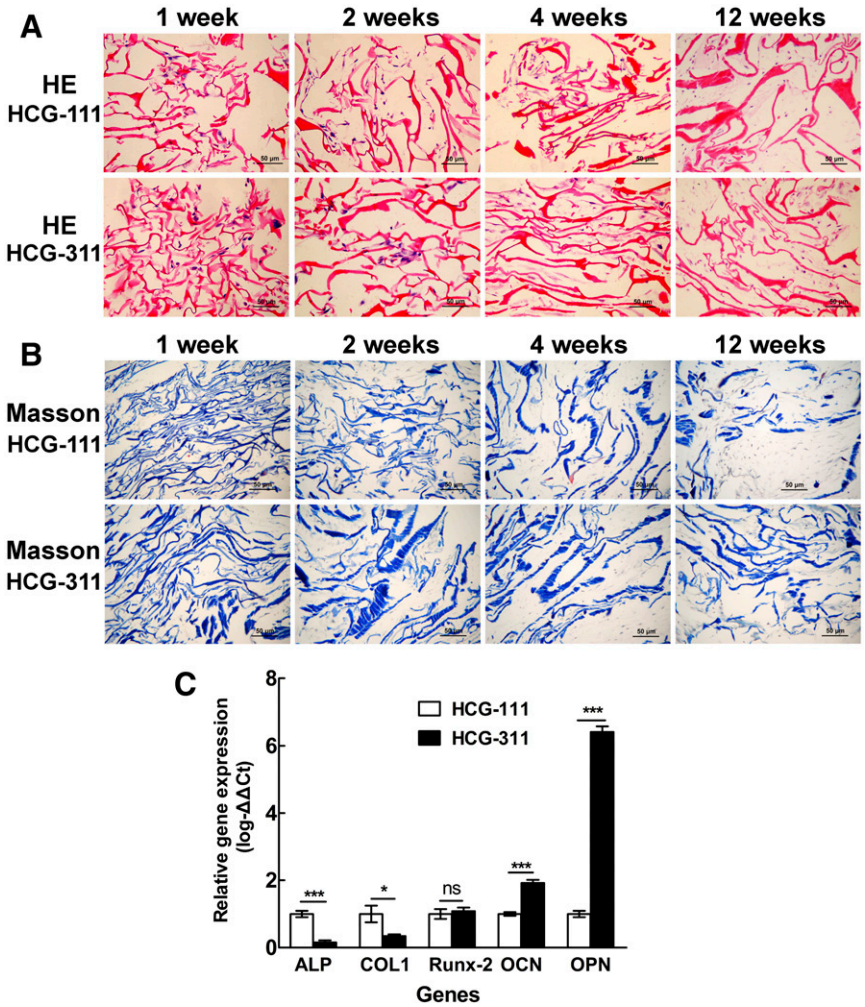

Figure 5. Histologic and quantitative real-time polymerase chain reaction (qRT-PCR) assessments of tissues cultured in vitro. Samples of human induced pluripotent stem cell (hiPSC)/nanohydroxyapatite/chitosan/gelatin (HCG) complexes were collected and sectioned for histologic staining at 1, 2, 4, and 12 weeks. **(A):** Sections were stained with H&E staining. The cells adhered and proliferated well on both HCG-111 and HCG-311 scaffolds. Dense extracellular matrix had formed at 12 weeks. Scale bars = 50 μm. **(B):** Sections were stained with Masson trichrome staining. Collagen stained in blue. Scale bars = 50 μm. **(C):** Bone-associated gene (*ALP*, *Col1*, *Runx-2*, *OCN*, and *OPN*) expression in hiPSCs on HCG-111 and HCG-311 scaffolds were analyzed by qRT-PCR at 4 weeks. The $2^{-\Delta\Delta Ct}$ method was used to analyze the results, where Ct values on HCG-311 were normalized to human 18S and further to the Ct values of the control HCG-111 samples. *OCN* and *OPN* expression in hiPSCs was significantly higher on HCG-311 scaffolds than on HCG-111 scaffolds ($p < .001$). Data are presented as mean $\pm$ SD ($n = 3$); *, $p < .05$; ***, $p < .001$. Abbreviations: HCG-111, nanohydroxyapatite/chitosan/gelatin scaffold with 1 wt/vol% nanohydroxyapatite; HCG-311, nanohydroxyapatite/chitosan/gelatin scaffold with 3 wt/vol% nanohydroxyapatite; ns, no statistically significant difference ($p > .05$).

influenced by the HA concentration, benefiting cell migration and tissue growth [35].

The appearance of the scaffolds (Fig. 3B) was almost the same when observed by the naked eye; however, the HCG-311 scaffold seemed tougher than the HCG-111 scaffold when cut with a blade. An open porous microstructure with a high degree of interconnectivity was generated in both HCG-111 and HCG-311 scaffolds by the phase separation and ice crystal sublimation process. HCG-111 had a larger pore width (51.1 $\pm$ 4.5 μm) than that of the HCG-311 (29.6 $\pm$ 3.9 μm), a statistically significant difference ($p < .001$; Fig. 3D). The SEM images at higher magnifications ($\times$1,000, $\times$5,000) showed the internal structure of the scaffolds. The HCG-111 scaffold had smoother pore walls than the HCG-311. The pore walls in the HCG-311 scaffolds contained more nodules approximately 2 μm. At the nanoscale ($\times$50,000), a much greater number of nHA particles was observed scattered on the surfaces of the HCG-311 than on the HCG-111 scaffolds (Fig. 3E).

Adsorption Characteristics in PBS and α-MEM (10% FBS)

Both HCG-111 and HCG-311 scaffolds have very high capability to uptake much more water and proteins from solutions than their self-weight. They performed differently in PBS and α-MEM (10% FBS) probably because α-MEM (10% FBS) contained much protein. In PBS (Fig. 3F), HCG-111 retained more water than did HCG-311. The mean weight percentage of the HCG-111 scaffolds increased sharply to the peak level of 230.9% at 1 week. Then, it gradually decreased to 166.9% at 12 weeks. In contrast, that of the HCG-311 scaffolds, after a fluctuation, reached a peak of 182.6% at 1 week. It had later decreased to 164.2% at 2 weeks and then plateaued. However, when soaked in α-MEM (10% FBS; Fig. 3G), HCG-311 showed more adsorption ability than

did HCG-111. The mean weight percentage of HCG-311 increased rapidly to a peak of 245.7% at 1 week. Afterward, it had decreased slightly at 3 weeks followed by an increase to 238.9% at 12 weeks. In contrast, for HCG-111, it had increased to 227.7% at 1 week, decreased to 175.8% at 3 weeks, and, finally, had increased to 225.3% at 12 weeks.

In Vitro Observation and Analysis of hiPSC/HCG Complex

The SEM images revealed that the hiPSCs attached and proliferated and an intercellular bridge had formed on both scaffolds at 4 weeks. After 12 weeks of cultivation, the outside surfaces of both complexes were covered with cells and extracellular matrix (ECM; Fig. 4B). However, a different appearance was observed inside the materials at 12 weeks. The pores in the HCG-311 scaffold appeared to have been filled with plenty of cells and ECM; however, in the HCG-111 scaffold, the cells had grown along the inside pore wall, and scaffold disintegration was observed (Fig. 4A).

H&E staining in Figure 5A showed that the hiPSCs had adhered and proliferated well, regardless of whether seeded on HCG-111 or HCG-311 scaffolds in vitro, with a denser matrix forming as time passed. However, the degradation of the HCG-111 scaffolds was much more than that of the HCG-311 scaffolds at 12 weeks, which was confirmed by Masson staining (Fig. 5B).

Bone-specific gene expression data are shown in Figure 5C, in which HCG-311 was compared with the HCG-111 control. The bone-associated gene (*OCN* and *OPN*) expression in hiPSCs was significantly higher on the HCG-311 scaffold ($p < .001$). In contrast, the expression of early markers (*ALP* and *Col1*) in hiPSCs on HCG-311 was significantly lower (*ALP*, $p < .001$; *Col1*, $p < .05$). Moreover, transcription factor Runx-2 expression had no obvious differences between the two scaffolds ($p > .05$).

In Vivo Evaluation of Composites in a Subcutaneous Implantation Model

After the CBCT data had been processed by the Software NNT viewer, the transplants and mouse bone and soft tissue were visualized from different perspectives (Fig. 6A, 6B). The Ct values of the samples in vitro, cultured for 12 weeks ($n = 3$), and in vivo, transplanted for 12 weeks ($n = 12$), were quantitatively calculated (Fig. 6C). In the in vitro cultivation, the mean Ct values had no significant differences among the groups ($p > .05$). However, in the in vivo transplantation, the mean Ct value of hiPSC/HCG-311 (1,363.5 $\pm$ 81.4 Hounsfield units [HU]) was significantly higher than that of hiPSC/HCG-111 (1,161.3 $\pm$ 79.8 HU; $p < .001$). Furthermore, these two values were not significantly different from the value of the mouse thighbone (1,260.7 $\pm$ 41.3 HU; $p > .05$).

The mice were sacrificed and transplants removed for analysis at 12 weeks (Fig. 6D). New bone formation was identified by histologic examination and IHC staining. In the pure scaffold group (Fig. 7A), the mouse cells had grown along the pore direction into the scaffolds, and collagen had formed. More cells and ECM were detected in the HCG-111 with a larger pore width. *RUNX-2* and *OCN* were weakly expressed on both scaffolds. In the hiPSC/scaffold group (Fig. 7B), H&E and Masson staining showed regenerated new bone-like tissue in vivo, in which bone lacunas containing osteocytes were seen and partially degraded scaffolds were also present. hiPSCs seeded on HCG-311 scaffolds generated large bone, and the hiPSCs seeded on HCG-111 scaffolds generated tiny bone. The in vivo-generated tissues were also

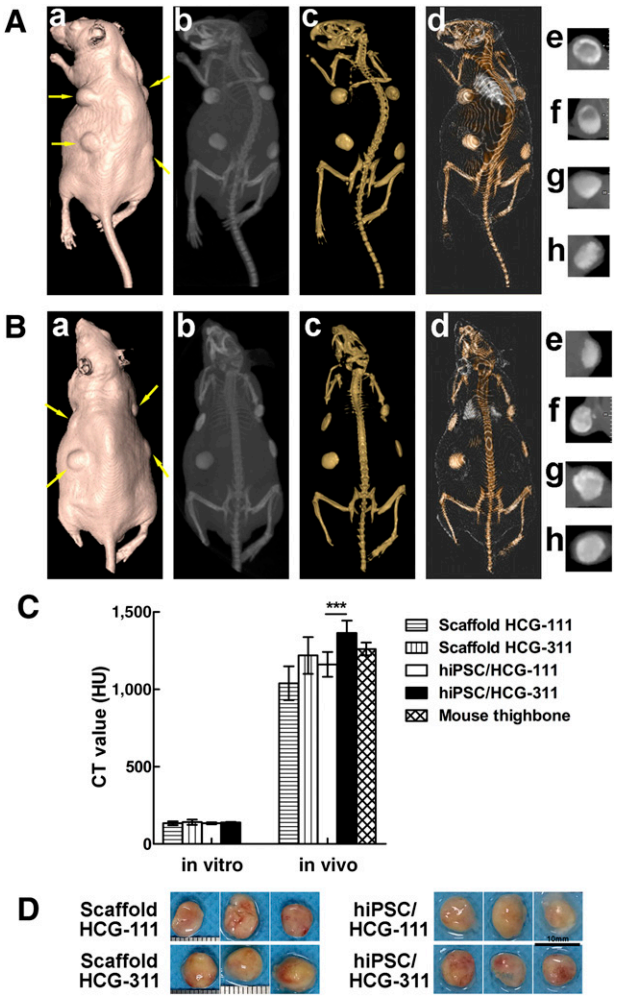

Figure 6. Cone-beam computed tomography (CBCT) imaging, analysis, and specimens of HCG-111 or HCG-311 alone or combined with hiPSCs subcutaneously transplanted into immunocompromised mice in vivo at 12 weeks. **(A):** Three-dimensional (3D) images of a mouse with pure scaffold transplants. Based on the CBCT data, 3D image creation of soft tissue **(Aa)**, maximum intensity projection (MIP) full-range visualization **(Ab)**, 3D rendering of materials at mouse bone density **(Ac)**, and bone plus soft tissue **(Ad)** were fabricated using the Software NNT viewer. Images of 0.5-mm-thick free-cut specimens were generated across the four implants (yellow arrows) individually, at upper left **(Ae)**, upper right **(Af)**, lower right **(Ag)**, and lower left **(Ah)**. The material in **(Ae, Af)** was HCG-111 and in **(Ag, Ah)** was HCG-311. **(B):** 3D imaging of mouse with hiPSC/scaffold complexes. Based on the CBCT data, 3D image creation of soft tissue **(Ba)**, MIP full-range visualization **(Bb)**, 3D rendering of materials at mouse bone density **(Bc)**, and bone plus soft tissue **(Bd)** were fabricated using the Software NNT viewer. Images of 0.5-mm-thick free-cut specimens were generated across the four implants (yellow arrows) individually, at upper left **(Be)**, upper right **(Bf)**, lower right **(Bg)**, and lower left **(Bh)**. The material in (Be, Bf) was hiPSC/HCG-111 and in **(Bg, Bh)** was hiPSC/HCG-311. **(C):** Ct value analysis was based on the bone density measurement tool in Software Mimics, version 10.01 (Materialise NV). Samples cultured in vitro for 12 weeks ($n = 3$) and transplanted in vivo for 12 weeks ($n = 12$) were quantitatively calculated, and mouse thigh bone sections ($n = 3$) were measured as the control. The Ct value of hiPSC/HCG-311 was significantly higher than that of hiPSC/HCG-111 in vivo. Data are presented as mean $\pm$ SD; ***, $p < .001$. **(D):** Photographs of specimens retrieved from mice at 12 weeks. Scale bars = 10 mm. Abbreviations: HCG-111, nanohydroxyapatite/chitosan/gelatin scaffold with 1 wt/vol% nanohydroxyapatite; HCG-311, nanohydroxyapatite/chitosan/gelatin scaffold with 3 wt/vol% nanohydroxyapatite; hiPSC, human induced pluripotent stem cell; HU, Hounsfield unit.

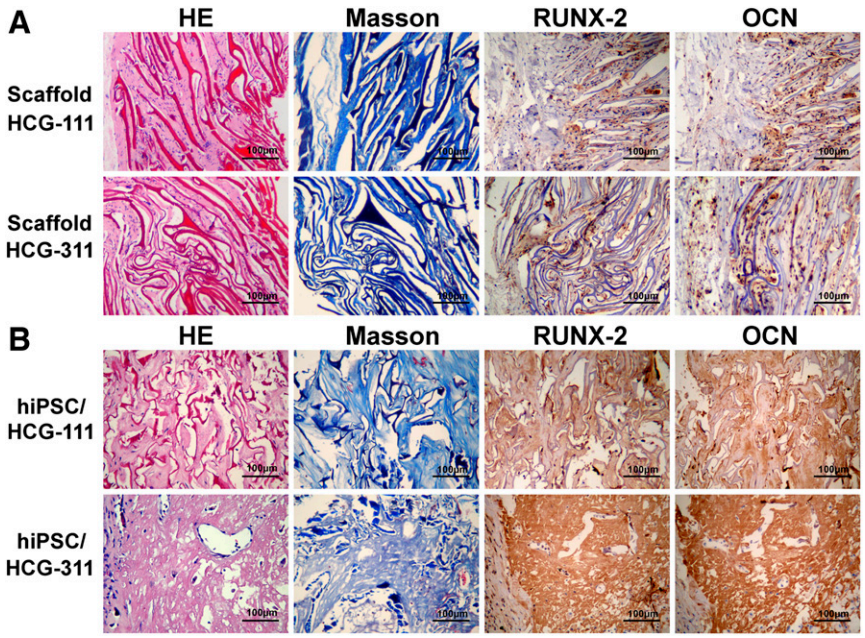

Figure 7. In vivo new bone formation was identified by histologic and immunohistochemistry (IHC) staining. HCG-111 or HCG-311 scaffolds alone or with human induced pluripotent stem cells (hiPSCs) were subcutaneously transplanted in immunocompromised mice at 12 weeks. **(A):** In the pure scaffold group, mouse cells grew along the pore direction into the scaffolds and collagen formed. More cells and extracellular matrix were detected in HCG-111 scaffolds with a larger pore width. *RUNX-2* and *OCN* were weakly expressed on both scaffolds. **(B):** In the hiPSC/ scaffold group, regenerated neotissue could be seen by HE and Masson staining, and partially degraded scaffolds were still present. On HCG-311 scaffolds, large amount of lacunas containing osteocytes formed within the bone-like matrix, and plenty of fiber-like structures could be seen on HCG-111 scaffolds. *RUNX-2* and *OCN* IHC-positive staining indicated that hiPSCs seeded on HCG-311 scaffolds generated mature bone and hiPSCs seeded on HCG-111 scaffolds generated little bone. Scale bars = 100 μm. Abbreviations: HCG-111, nanohydroxyapatite/chitosan/ gelatin scaffold with 1 wt/vol% nanohydroxyapatite; HCG-311, nanohydroxyapatite/chitosan/gelatin scaffold with 3 wt/vol% nanohydroxyapatite; HE, H&E; hiPSC, human induced pluripotent stem cell.

resected for anti-*RUNX-2* and anti-*OCN* IHC staining. The results showed that *RUNX-2* and *OCN* were highly expressed in bone generated on HCG-311 scaffolds but were weakly expressed in tissues formed on HCG-111 scaffolds.

Discussion

Bone tissue engineering has provided a new promising method for bone regeneration; however, to date, the most suitable scaffolds and cell sources still require research [10, 38]. iPSCs resulted in great potential for application in bone regeneration alternatives. In the present study, we successfully isolated hGFs from clinical discarded gingival tissues and established hiPSCs from hGFs. In addition, we fabricated HCG scaffolds with two different HA ratios to perform osteogenic induction. The results demonstrated that HCG-311 scaffolds improved osteogenic differentiation of hiPSCs from hGFs in vitro and in vivo; therefore, our results suggest a promising cell source candidate and a potential innovative technique for bone tissue engineering.

As cell sources, ESCs and adult stem cells have their advantages and disadvantages. ESCs have pluripotent differentiation capability; however, ethical problems exist. In contrast, adult stem cells do not generate ethical concerns; however, they have a limited lifespan, resulting in insufficient cells for bone tissue engineering. iPSCs were developed in 2006 [12] and soon became popular in fields such as genetic disease cell models and regenerative medicine as a cell source [13–17]. iPSCs have ESC characteristics, and ethical problems can probably be avoided, because iPSCs have been reprogrammed from the patient's own somatic cells. In theory, iPSCs can generate all tissues and organs, the same as ESCs. A few research groups have reported that different tissues were generated using iPSCs, and hiPSCs have already been used in clinical therapy [39–41]. hiPSCs from hGFs proved to have weak osteogenesis capability, probably because of the epigenetic memory [42, 43]. However, patient hGFs were isolated from easily obtainable discarded gingival tissues in the dental clinic. This ability was interesting and promising enough that we determined whether they could useful for bone regeneration. In our study, hGFs were successfully developed and reprogrammed into hiPSCs for further osteogenic differentiation experiments. The results showed that hGFs have weak osteogenic differentiation capability; the ability had almost disappeared by passage 10. However, for hiPSCs, the osteogenic differentiation capability was almost the same at passages 2, 5, and 10. This finding suggests that when hGFs are reprogrammed into hiPSCs, the osteogenic differentiation capability increases greatly. The explanation might be that iPSCs are in an earlier cell stage and thus can easily differentiate into osteoblasts.

The currently available bone tissue engineering scaffolds can generally be divided into nondegradable and degradable [44–46]. Nondegradable bone scaffolds include titanium, ceramics, and so forth. The degradable scaffolds contain HA, chitosan, collagen, gelatin, poly(lactic-co-glycolic acid) [47, 48], and others. Because a combination of degradable scaffolds will best mimic the natural bone components, the HCG composite has served as one of the favorite scaffolds for bone regeneration.

In the present study, the ratio of solid components (nHA, chitosan, and gelatin) was 3:1:1, resulting in 60% nHA in relative weight (nHA content in natural bone, 50%–70% [49]). The findings showed that the different nHA ratios influenced the morphology, porosity, and adsorption characteristics of the HCG scaffolds. Our work has indicated that HCG-311 can better induce osteogenesis of hiPSCs from hGFs in vitro, and new bone was generated when hiPSCs and HCG-311 composites were transplanted in vivo. The possible reasons are as follows. First, as an inorganic reinforcement, the nHA in the composite largely enhanced the mechanical properties with high strength and toughness. Second, the close association and direct chemical bonding of the inorganic (hydroxyapatite) crystallites and polymer (chitosan and gelatin) in the HCG matrices limit the ability of the HA nanoparticles to migrate away, resulting in considerable bioactivity improvement, increased protein and calcium adsorption and decreased composite degradation [23]. Finally, in a nonreceptor-mediated fashion, nHA can easily translocate into the cytoplasm through the cell membrane [50]. Used as a chemical factor, nHA promoted cell viability and proliferation and osteogenic differentiation [51, 52]. In the present study, hiPSCs from hGFs had almost no bone formation capability, even when combined with bone-inducing scaffolds. However, HCG-311 scaffolds significantly increased the osteogenic differentiation capability of hiPSCs from hGFs in vitro and in vivo. It has been hypothesized that HCG-311 scaffolds induce bone-associated gene expression during the osteogenesis-inducing process of hiPSCs from hGFs [53]; further investigation is ongoing regarding the more mechanistic details. Studies of large animal models using techniques from these cited studies and safer reprogramming methods such as using proteins and small molecules to confirm the results is underway.

Conclusion

The present study focused on patient-personalized bone tissue engineering. We established hiPSCs from patient hGFs isolated from easily obtainable discarded gingival tissues in a dental clinic. We also developed a new approach for better osteogenetic efficiency of hiPSCs derived from hGFs combined with defined HCG scaffolds. It is an innovative and promising approach for large bone regeneration, although more investigations should be performed before clinical use.

Acknowledgments

This work was supported by the National Natural Science Foundation of China (Grant 81200770), Natural Science Foundation of Jiangsu Province, China (Grant BK20130081), and Jiangsu Provincial Clinical Medicine of Science and Technology project (Grants BL2012017 and BL2013005). The project was also funded by the Medical Science and Technology Development Foundation, Nanjing Department of Health (Grant YKK12123).

Author Contributions

J.J.: manuscript writing, collection and/or assembly of data, data analysis and interpretation; X.T. and X.H.: collection and/or assembly of data, data analysis and interpretation; J.Z.: provision of study material or patients, administrative support; H.Q. and Q.H.: conception and design, manuscript editing, final approval of manuscript.

Disclosure of Potential Conflicts of Interest

The authors indicated no potential conflicts of interest.

References

1 Spector M. Biomaterials-based tissue engineering and regenerative medicine solutions to musculoskeletal problems. Swiss Med Wkly 2006;136:293–301.

2 Ikada Y. Tissue Engineering: Fundamentals and Applications. Amsterdam; Elsevier, 2006.

3 Steinert AF, Rackwitz L, Gilbert F et al. Concise review: The clinical application of mesenchymal stem cells for musculoskeletal regeneration: Current status and perspectives. Stem Cells Translational Medicine 2012;1:237–247.

4 Testa G, Harris J. Genetics: Ethical aspects of ES cell-derived gametes. Science 2004;305: 1719.

5 Pittenger MF, Mackay AM, Beck SC et al. Multilineage potential of adult human mesenchymal stem cells. Science 1999;284:143–147.

6 Uccelli A, Pistoia V, Moretta L. Mesenchymal stem cells: A new strategy for immunosuppression? Trends Immunol 2007;28:219–226.

7 Caplan AI. Adult mesenchymal stem cells for tissue engineering versus regenerative medicine. J Cell Physiol 2007;213:341–347.

8 Liu Y, Wang L, Kikuiri T et al. Mesenchymal stem cell-based tissue regeneration is governed by recipient T lymphocytes via IFN-γ and TNF-α. Nat Med 2011;17:1594–1601.

9 Yan X, Qin H, Qu C et al. iPS cells reprogrammed from human mesenchymal-like stem/progenitor cells of dental tissue origin. Stem Cells Dev 2010; 19:469–480.

10 Ko JY, Kim KI, Park S et al. In vitro chondrogenesis and in vivo repair of osteochondral defect with human induced pluripotent stem cells. Biomaterials 2014;35:3571–3581.

11 Egusa H, Kayashima H, Miura J et al. Comparative analysis of mouse-induced pluripotent stem cells and mesenchymal stem cells during osteogenic differentiation in vitro. Stem Cells Dev 2014;23:2156–2169.

12 Takahashi K, Yamanaka S. Induction of pluripotent stem cells from mouse embryonic and adult fibroblast cultures by defined factors. Cell 2006;126:663–676.

13 Takahashi K, Tanabe K, Ohnuki M et al. Induction of pluripotent stem cells from adult human fibroblasts by defined factors. Cell 2007; 131:861–872.

14 Yu J, Vodyanik MA, Smuga-Otto K et al. Induced pluripotent stem cell lines derived from human somatic cells. Science 2007;318: 1917–1920.

15 Kim JB, Sebastiano V, Wu G et al. Oct4-induced pluripotency in adult neural stem cells. Cell 2009;136:411–419.

16 Shi Y, Do JT, Desponts C et al. A combined chemical and genetic approach for the generation of induced pluripotent stem cells. Cell Stem Cell 2008;2:525–528.

17 Shi Y, Desponts C, Do JT et al. Induction of pluripotent stem cells from mouse embryonic fibroblasts by Oct4 and Klf4 with small-molecule compounds. Cell Stem Cell 2008;3: 568–574.

18 Mastrogiacomo M, Muraglia A, Komlev V et al. Tissue engineering of bone: Search for a better scaffold. Orthod Craniofac Res 2005;8:277–284.

19 Shin M, Yoshimoto H, Vacanti JP. In vivo bone tissue engineering using mesenchymal stem cells on a novel electrospun nanofibrous scaffold. Tissue Eng 2004;10:33–41.

20 Park JS, Yang HN, Woo DG et al. In vitro and in vivo chondrogenesis of rabbit bone marrow-derived stromal cells in fibrin matrix mixed with growth factor loaded in nanoparticles. Tissue Eng Part A 2009;15:2163–2175.

21 Chen J, Chen H, Li P et al. Simultaneous regeneration of articular cartilage and subchondral bone in vivo using MSCs induced by a spatially controlled gene delivery system in bilayered integrated scaffolds. Biomaterials 2011;32:4793–4805.

22 Zhao F, Yin Y, Lu WW et al. Preparation and histological evaluation of biomimetic three-dimensional hydroxyapatite/chitosan-gelatin network composite scaffolds. Biomaterials 2002;23: 3227–3234.

23 Zhao F, Grayson WL, Ma T et al. Effects of hydroxyapatite in 3-D chitosan-gelatin polymer network on human mesenchymal stem cell construct development. Biomaterials 2006;27: 1859–1867.

24 Isikli C, Hasirci V, Hasirci N. Development of porous chitosan-gelatin/hydroxyapatite composite scaffolds for hard tissue-engineering applications. J Tissue Eng Regen Med 2012;6: 135–143.

25 Clauss M, Furustrand Tafin U, Betrisey B et al. Influence of physico-chemical material characteristics on staphylococcal biofilm formation—A qualitative and quantitative in vitro analysis of five different calcium phosphate bone grafts. Eur Cell Mater 2014;28:39–50.

26 Gleeson JP, Plunkett NA, O'Brien FJ. Addition of hydroxyapatite improves stiffness, interconnectivity and osteogenic potential of a highly porous collagen-based scaffold for bone tissue regeneration. Eur Cell Mater 2010;20: 218–230.

27 Shi Z, Huang X, Cai Y et al. Size effect of hydroxyapatite nanoparticles on proliferation and apoptosis of osteoblast-like cells. Acta Biomater 2009;5:338–345.

28 Li J, Chen Y, Yin Y et al. Modulation of nano-hydroxyapatite size via formation on chitosan-gelatin network film in situ. Biomaterials 2007;28:781–790.

29 Rajkumar M, Kavitha K, Prabhu M et al. Nanohydroxyapatite-chitosan-gelatin polyelectrolyte complex with enhanced mechanical and bioactivity. Mater Sci Eng C 2013;33:3237–3244.

30 Thein-Han WW, Misra RD. Biomimetic chitosan-nanohydroxyapatite composite scaffolds for bone tissue engineering. Acta Biomater 2009;5:1182–1197.

31 Liao S, Ngiam M, Chan CK et al. Fabrication of nano-hydroxyapatite/collagen/osteonectin composites for bone graft applications. Biomed Mater 2009;4:025019.

32 Qin H, Qu C, Yamaza T et al. Notice of retraction of "Ossifying fibroma tumor stem cells are maintained by epigenetic regulation of a TSP1/TGF-β/SMAD3 autocrine loop" [retraction of: Qin H, Qu C, Yamaza T et al. In: Cell Stem Cell 2013;13:577–589]. Cell Stem Cell 2015;16: 569.

33 Johari N, Fathi MH, Golozar MA et al. Poly (ε-caprolactone)/nano fluoridated hydroxyapatite scaffolds for bone tissue engineering: In vitro degradation and biocompatibility study. J Mater Sci Mater Med 2012;23:763–770.

34 Yang J, Shi G, Bei J et al. Fabrication and surface modification of macroporous poly(L-lactic acid) and poly(L-lactic-co-glycolic acid) (70/30) cell scaffolds for human skin fibroblast cell culture. J Biomed Mater Res 2002;62:438–446.

35 Chang KH, Liao HT, Chen JP. Preparation and characterization of gelatin/hyaluronic acid cryogels for adipose tissue engineering: In vitro and in vivo studies. Acta Biomater 2013;9: 9012–9026.

36 El-Gendy R, Yang XB, Newby PJ et al. Osteogenic differentiation of human dental pulp stromal cells on 45S5 Bioglass® based scaffolds in vitro and in vivo. Tissue Eng Part A 2013;19: 707–715.

37 Livak KJ, Schmittgen TD. Analysis of relative gene expression data using real-time quantitative PCR and the 2(-Delta Delta C(T)) method. Methods 2001;25:402–408.

38 Hutmacher DW. Scaffolds in tissue engineering bone and cartilage. Biomaterials 2000; 21:2529–2543.

39 Robinton DA, Daley GQ. The promise of induced pluripotent stem cells in research and therapy. Nature 2012;481:295–305.

40 Ko JY, Im GI. Chondrogenic and osteogenic induction from iPS cells. Methods Mol Biol 2014;.

41 Tashiro K, Inamura M, Kawabata K et al. Efficient adipocyte and osteoblast differentiation from mouse induced pluripotent stem cells by adenoviral transduction. STEM CELLS 2009;27: 1802–1811.

42 Hynes K, Menicanin D, Mrozik K et al. Generation of functional mesenchymal stem cells from different induced pluripotent stem cell lines. Stem Cells Dev 2014;23:1084–1096.

43 Kim K, Doi A, Wen B et al. Epigenetic memory in induced pluripotent stem cells. Nature 2010;467:285–290.

44 Zong C, Xue D, Yuan W et al. Reconstruction of rat calvarial defects with human mesenchymal stem cells and osteoblast-like cells in poly-lactic-co-glycolic acid scaffolds. Eur Cell Mater 2010;20:109–120.

45 Fiorilli S, Baino F, Cauda V et al. Electrophoretic deposition of mesoporous bioactive glass on glass-ceramic foam scaffolds for bone tissue engineering. J Mater Sci Mater Med 2015;26:5346.

46 Nandi SK, Kundu B, Mahato A et al. In vitro and in vivo evaluation of the marine sponge skeleton as a bone mimicking biomaterial. Integr Biol (Camb) 2015;7:250–262.

47 Luangphakdy V, Shinohara K, Pan H et al. Evaluation of rhBMP-2/collagen/TCP-HA bone graft with and without bone marrow cells in the canine femoral multi defect model. Eur Cell Mater 2015;29:57–68; discussion 68–69.

48 Lou T, Wang X, Song G et al. Structure and properties of PLLA/β-TCP nanocomposite scaffolds for bone tissue engineering. J Mater Sci Mater Med 2015;26:5366.

49 Clarke B. Normal bone anatomy and physiology. Clin J Am Soc Nephrol 2008;3(suppl 3):S131–S139.

50 Bodakhe S, Verma S, Garkhal K et al. Injectable photocrosslinkable nanocomposite based on poly(glycerol sebacate) fumarate and hydroxyapatite: Development, biocompatibility and bone regeneration in a rat calvarial bone defect model. Nanomedicine (Lond) 2013;8:1777–1795.

51 Saiz E, Zimmermann EA, Lee JS et al. Perspectives on the role of nanotechnology in bone tissue engineering. Dent Mater 2013;29:103–115.

52 Stevens MM, George JH. Exploring and engineering the cell surface interface. Science 2005;310:1135–1138.

53 Kang JS, Alliston T, Delston R et al. Repression of Runx2 function by TGF-beta through recruitment of class II histone deacetylases by Smad3. EMBO J 2005;24:2543–2555.

See www.StemCellsTM.com for supporting information available online.

